Experimental and analytical study on heat generation characteristics of a lithium-ion power battery

Yongqi Xie[a,*], Jincheng Tang[a], Shang Shi[b], Hongwei Wu[c,], Jianzu Yu[a]**

[a]School of Aeronautic Science and Engineering, Beihang University, Beijing, 100191, China

[b]The 55th Research Institute, China Electronics Technology Group Corporation, Nanjing, 210016, China

[c]School of Engineering and Technology, University of Hertfordshire, Hatfield, AL10 9AB, United Kingdom

[*]Corresponding author: Tel: +86(10) 8233 8081, Fax.: +86(10) 8233 8952, E-mail: xyq@buaa.edu.cn

**Corresponding author: Tel.: +44(0)1707 284265, Fax.: +44(0)1707 285086, E-mail: h.wu6@herts.ac.uk

Abstract: In this article, a combined experimental and analytical study has been performed to investigate the transient heat generation characteristics of the lithium-ion power battery. An experimental apparatus is newly built and the investigations on the charge/discharge characteristics and temperature rise behavior are carried out at the ambient temperatures of 28 °C, 35 °C and 42 °C over the period of 1C, 2C, 3C and 4C rates. The thermal conductivity of a single battery cell is measured, which is 5.22 W/(m·K). A new model of the heat generation rate based on the battery air cooling system is proposed by the lumped parameter approach. Comparison between the simulated battery temperatures with experimental data is performed and good agreement is achieved. The impacts of the ambient temperature and charge/discharge rates on the heat generation rate are further analyzed. It is found that both ambient temperature and charge/discharge rates have significant influences on the voltage change and temperature rise as well as heat generation rate. During charge/discharge, the larger the current rate, the larger the heat generation rate. The effect of the ambient temperature on the heat generation shows an obvious difference with different state of charge.

Keywords: Lithium-ion battery; heat generation model; heat generation rate; temperature rise; thermal management system

Nomenclature

B	time constant, s
Bi	Biot number
c	specific heat capacity, J/(kg·K)
E	open-circuit potential, V
h	convective heat transfer coefficient, W/(m^2·K)
I	current, A
l	characteristic length, m
q	heat generation rate of battery, W
Q	rate of heat generated or consumed, J
R	thermal resistance, K/W
T	temperature, K
t	time, s
U	terminal voltage, V
V	volume, m^3
x, y, z	coordinate direction vector
ΔT	Temperature rise, K

Greek symbols

λ	Thermal conductivity, W/(m·K)
ρ	Density, kg/m^3
τ	time step, s

Subscripts

amb	ambient
h	convection heat transfer
J	Joule heat
max	maximum
t	time
v	volume

Acronyms

DC	direct current
DOD	depth of discharge
EV	electric vehicle
HEV	hybrid electric vehicle
ITMS	integrate thermal management system
TMS	thermal management system
TPS	transient plane source
SOC	state of charge

1. Introduction

Among the electrochemical energy storage systems, lithium-ion batteries, as a promising candidate, have attracted considerable attention in many power demand applications due to their advantages of large specific energy, high power density, charge/discharge cycle stability and long cycle lifetime [1, 2]. With rapid development of the electric vehicles (EVs) and hybrid electric vehicles (HEVs), lithium-ion batteries have been widely used in recent years [3]. However, a large amount of heat will be generated because of the electrochemical reactions and physical changes inside the batteries, potentially bringing out capacity fade and thermal runaway [4]. Therefore, it is crucial to have insight into the heat generation characteristics for maintaining safety and performance of the battery.

Many researches on the safety issues of the battery are finally ascribed to the heat generation and heat dissipation at each level of the battery system [5, 6]. In order to keep the battery within a reasonable temperature, an efficient thermal management system (TMS) will be needed to dissipate the heat generated. Furthermore, the heat generation rate is a necessary prerequisite for an efficient TMS design [7, 8]. Therefore, it is imperative to understand the mechanism of the battery heat generation characteristics and its effect on the battery performance.

A number of researchers have been devoted to dealing with the thermal models to determine the temperature distributions of the battery cell over the past three decades. Bernardi et al. [9] firstly developed a general thermal model on the basis of the energy balance for the battery systems. They considered that the cell temperature resulted from the interaction of the Joule heat,

heat of mixing, phase-change heat and electrochemical reaction heat with component-dependent open-circuit potentials. The heat generation rate could be calculated as the temperature was assumed to be uniform throughout and varied with time. Afterwards, Rao and Newman [10] presented a simplified thermal model to determine the rate of the heat generation for insertion battery systems. In their study, the effects of the mixing heat and phase-change heat were neglected. Utilizing the thermal model proposed by Bernardi et al [9], the battery thermal behavior was studied by Dong and Baek [11]. It was found that the irreversible Joule heat dominated under high-rate discharge conditions, but the reversible entropic heat from electrochemical reactions account for the main part under low-rate discharge conditions. Forgez et al. [12] developed a lumped parameter thermal model of a cylindrical lithium-ion battery considering the heat generated from resistive dissipation and the reversible entropic heat as the heat generation of the battery. And the internal and external resistances of the battery were calculated by a steady state method. For the heat generation, Sato [13] and Lai et al. [14] considered three different heat, which were electrochemical reaction heat, polarization heat and Joule heat. The level of the heat generated was a result of the attribution from each heat. They also investigated the variation of the irreversible and reversible heat production as a function of the depth of discharge (DOD) [14]. For a prismatic lithium-ion battery cell, Greco et al. [13] developed a simplified one-dimensional transient thermal network model using thermal circuit method linked with the thermal model of the heat pipe. In order to validate the model, they also presented a special one-dimensional analytical model and a three-dimensional simulation model. The heat generation rate in a battery cell was determined by adopting the model shown in Ref. [14]. The results showed that the thermal network model was sufficient to predict the battery temperature distribution. Combining an analytical solution of the lumped capacitance model and thermography, Bazinski and Wang [15] calculated the rate of the heat generated inside a pouch lithium-ion battery under different rates. The internal uniform heat generation was assumed and expressed by a simple third order polynomial. However, some profile shapes of the heat would defy being accurately modeled by a polynomial in despite of its order. Yildiz et al. [15] proposed a thermal model for a pouch lithium-ion battery only accounting for the irreversible Joule heat. The battery temperature rises calculated by the model demonstrated an identical behavior with experimental results. A simplified model of heat generation can be used to calculate the rate in constant current discharge process. Birgersson et al. [16] developed a two-dimensional transient mathematical model and studied the heat generation characteristics of 18650 cylinder lithium-ion battery pack. It was reported that in normal discharge process the ohmic heat dominated at low-rate discharge but the reversible electrochemical heat dominated at high-rate discharge. Lin et al. [17] formulated a coupled electro-thermal model for cylindrical battery. The electrical model calculated the battery state of the charge (SOC) and voltage. The heat generation was determined by the difference between the terminal voltage and open circuit voltage, along with the current. A two-state model was used to capture the lumped thermal dynamics of the battery. Among these above thermal models, accurately determining the heat generation of the battery was crucial for accurate prediction of the temperature distribution.

In the aspect of studies on the heat generation rate, a comprehensive review was perfectly performed by Bandhauer et al. [18]. In the literature, there are mainly three methods to determine the rate of the heat generation, which are directly experimental measurement, prediction using Bernardi model and relevant experimental data, as well as prediction using electro-thermal model. Some existing experimental measurements mainly focus on the heat generation by accelerated-rate calorimetry and isothermal heat conduction calorimetry [18-21], or by measuring the overpotential and entropic heat coefficient [22]. Hallaj et al. [18] studied the heat generation characteristics of the commercial lithium-ion battery according to electrochemical calorimeter. The internal resistance and entropic change coefficient at different depth of discharges (DODs) were measured. The results showed that there was obvious endothermic phenomenon during the charge, owing to entropic heat more than Joule heat. However, the heat generation rate was always positive in the discharge process. Balasundaram et al. [20] measured the total heat generation of 18650 cell under different charge and discharge rates conditions by accelerated-rate calorimetry. For the irreversible heat generation, the intermittent pulse technique was used and the reversible heat generation was obtained from the determination of the entropic coefficient at different SOC and DOD. They found that the reversible heat was primary at lower current rates, which should be taken into account as building thermal model. Saito [21] carried out an experimental study on the thermal behaviors of the lithium-ion batteries during high-rate pulse cycling and measured the rate of heat generation using calorimeter method. It was found that the additional heat in high-rate pulse discharge process usually resulted from side reaction, which changed the surface characteristics of the electrode and increased the impedance. Yasir et al. [19] experimentally investigated the heat generation in high power prismatic lithium-ion battery cell. The heat generation rate was calculated by measuring the overpotential resistances with four different methods and entropic heat generated in the cell. Calorimeter tests were also carried out to compare the calculated and measured heat generation. Bandhauer et al. [23] measured the temperature-dependent electrochemical heat generation for a commercial lithium-ion battery. It was found that the total heat generation was a strong function of temperature, current and DOD. The heat rate increased as the rate increased and the temperature decreased simultaneously. The entropic heating in the dynamic simulation was significant, especially in a charge depletion dynamic profile. Damay et al. [22] proposed thermal and heat generation models for large prismatic lithium-ion cell. The model parameters were experimentally determined and the irreversible Joule heat was measured by galvanostatic intermittent titration technique. The reversible electrochemical reaction heat was obtained through measuring the entropic coefficient. Panchal et al. [24] presented a method of measuring heat generation rate based on the battery temperature and heat flux. The discharge rate was 1C, 2C, 3C and 4C and the ambient temperature was 5 ^{o}C, 15 ^{o}C, 25 ^{o}C and 35 ^{o}C, respectively. The results showed that the heat generation rate increased as the discharge rates increased. The variations of the ambient temperature and increase in discharge rate have a great impact on the discharge capacity. In addition, they [25] also developed a mathematical model to calculate the transient temperature distributions for a large sized prismatic lithium-ion battery under different current rates conditions. Infrared radiation images of the battery cooled by ambient air were taken at 1C, 2C, 3C and 4C discharge rates. It was found that the increased current rates caused the battery surface temperatures increasing.

In thermal models, heat generation of the battery is usually considered as the sum of reversible and irreversible heat [10-12, 16, 23-27]. The related equation presented by Bernardi et al. [9] is mainly used to calculate the heat generation. The temperature rise of the battery is generally a transient behavior. To get the transient heat generation rate over the charge and discharge period will be very helpful for addressing the battery temperature rise behavior of each thermal management strategy. Despite numerous researches on thermal modeling have been carried out, to the best of author’s knowledge, relatively few papers have dealt with the transient heat generation characteristics of the battery and the effects of such as ambient temperature, charge and discharge rates. Therefore, the current work was motivated by the requirement to develop a reliable and possibly simple approach to determine the transient rate of the heat generation for large pouch battery cell. Another main contribution could be to investigate the transient heat generation characteristics of the battery under high charge/discharge rate and wide temperature range conditions and the effects of different control factors such as ambient temperature, charge and discharge rates.

In this article, the heat generation characteristics of the lithium-ion power battery will be investigated from both experimental and theoretical aspects. First, an experimental apparatus of battery heat generation characteristics will be setup and the heat generation characteristics will be explored in detail. Second, both models of heat generation and heat dissipation are described in terms of air cooling system and the expression for estimating the transient heat generation rate is developed based on the energy balance and corresponding temperature data measured. Finally, the impacts of the ambient temperature and charge/discharge rate on the battery charge/discharge characteristics, temperature rise behavior and heat generation rate are discussed.

2. Experimental setup

A new experimental apparatus was set up at Human-Machine and Environmental Engineering Laboratory at Beihang University, China to study the heat generation characteristics of the power battery.

2.1 Battery thermal conductivity test device

Hot Disk Analyzer (TPS 1500) based on transient plane source (TPS) method was used to measure the thermal conductivity of the battery cell. The principle of the TPS method was to add the heat interference to the heat balance sample, and then recorded the temperature response of the sample to the heat interference [28]. Moreover, thermal property parameter values could be determined according to the transient temperature response of an infinite medium during step heating. Fig. 1 shows the test device including a constant current power supply, voltage test unit, Wheatstone bridge and the Hot Disk probe (model 4922).

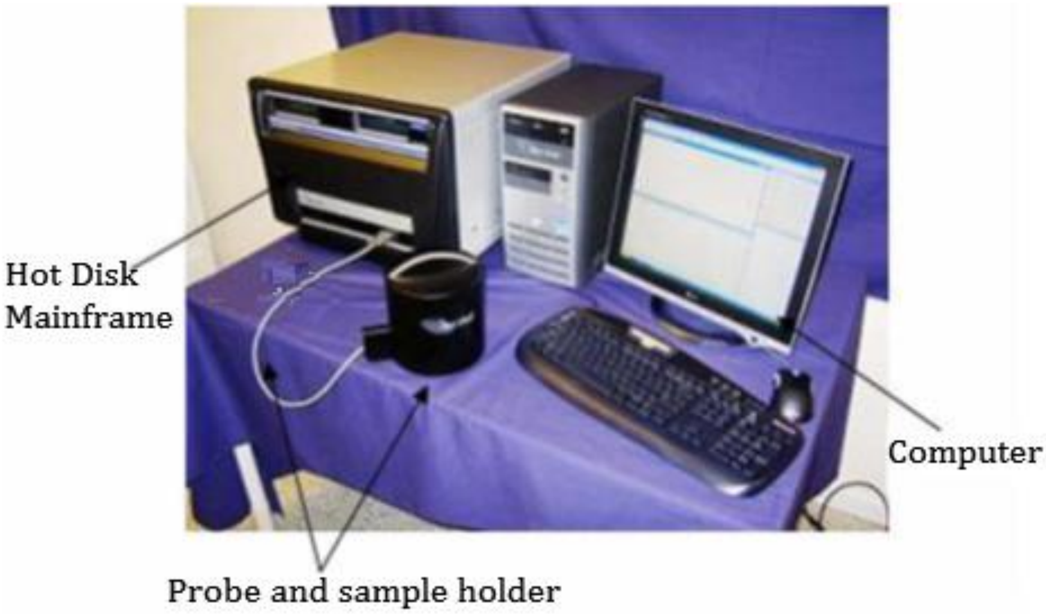

Fig. 1. Thermal conductivity of the battery test device.

In the current study, as the thickness of a single battery cell was 6.1 mm, four cells were stacked to meet the requirement of the sample size. The probe was placed in the middle of the cells to form a sandwich structure. In order to reduce the thermal contact resistance, the samples were compressed tightly. A seal cover was used to cover the samples to avoid the impact of the surroundings. The heating power was 0.5 W with 20 s heating duration at the room temperature of 24.0 ^{o}C. Repeat measurements were carried out and the arithmetic average value of the thermal conductivity was adopted.

2.2 Heat generation characteristics experimental apparatus

The schematic of the experimental apparatus and the sample of the battery cells are shown in Fig. 2. The system mainly consists of the charge and discharge subsystem, the thermal performance test subsystem and the data acquisition subsystem. In the thermal performance test subsystem, the thermostatic chamber (QGT302P) with the temperature ±0.5 ^{o}C was utilized to simulate different ambient temperatures. Three different chamber temperatures of 28 ^{o}C, 35 ^{o}C and 42 ^{o}C were selected in the experiment. The battery cells arranged inside the porous structure frame were vertically placed in the thermostatic chamber and could be preheated prior to the formal test. The data acquisition subsystem mainly included an Agilent 34970A, platinum temperature sensors (PT100, ±0.06 ^{o}C at 0 ^{o}C) and a computer. Two PT100 probes were affixed on the surface of the cell and the temperatures were recorded every second by the Agilent 34970A. The arithmetic average of both PT100 was considered as the cell surface temperature.

The charge and discharge of the battery at rates of 1C/10A, 2C/20A, 3C/30A and 4C/40A were accomplished by the charge and discharge subsystem. During the charge period, the battery was first charged at constant current (1C, 2C, 3C and 4C) to a voltage of 2.8 V. Thereafter, the voltage was kept at 2.8 V and taper-charged to 0.05 A. While during the discharge period, the battery was discharged at constant (1C, 2C, 3C and 4C) to a voltage of 1.5 V. The basic parameters of the commercial battery cell properties are listed in Table 1.

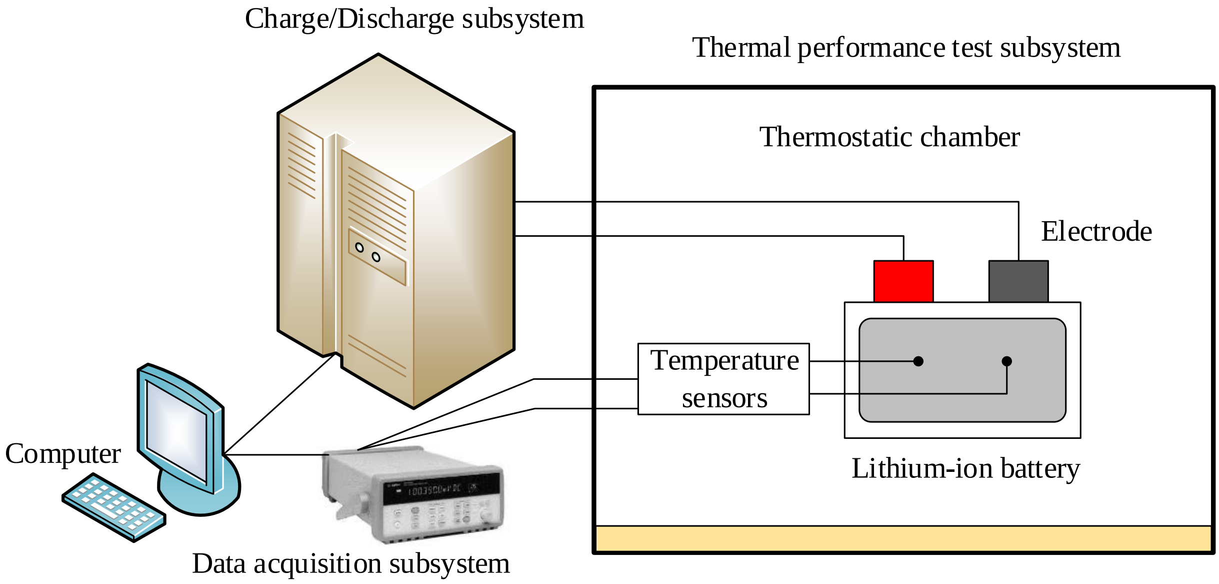

(a) Schematic of the experimental apparatus

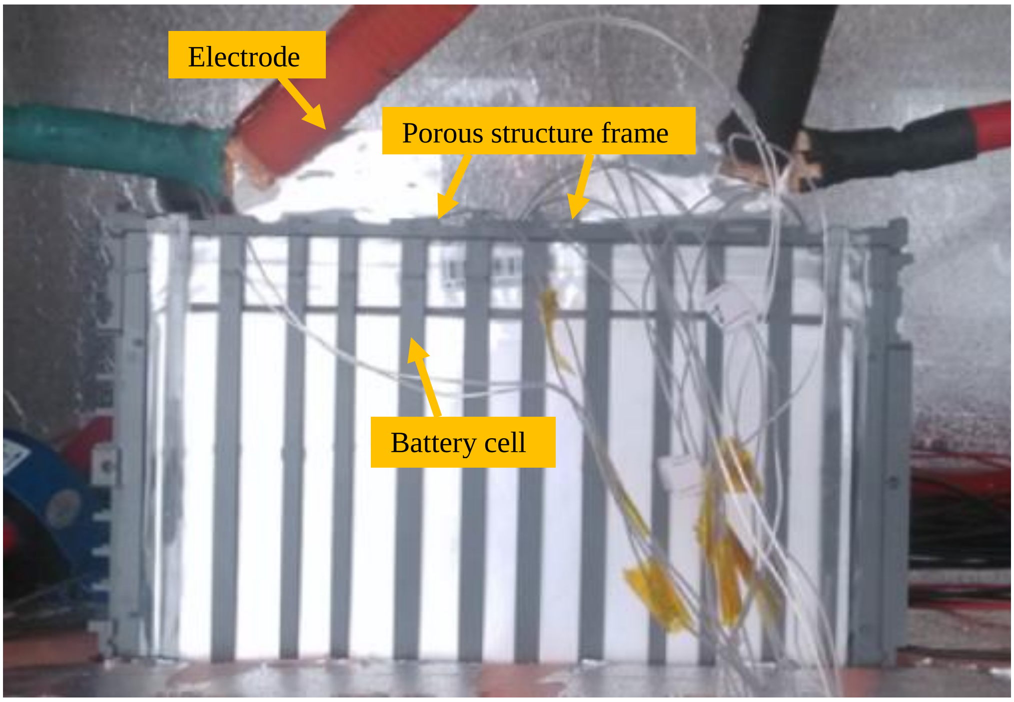

(b) The sample of battery cells

Fig. 2. Schematic of the experimental apparatus and the sample of battery cells.

Table 1 Parameters of commercial battery cell.

Specifications	Value (unit)
Type	Lithium-ion titanate battery
Dimensions	0.0061 m×0.203 m×0. 127 m
Nominal voltage	2.3 V
Nominal capacity	10 A h
Recommended operation temperature	-10 ~ +45 ºC (charge)
	-25 ~ +55 ºC (discharge)

The testing procedure was as the following. The given ambient temperature was firstly simulated by the thermal performance test subsystem. After the steady state in the thermostatic chamber reached, the charge and discharge tests were carried out. Simultaneously, the data of temperatures, currents and voltages were collected and recorded by the data acquisition subsystem.

3. Thermal model

3.1. Heat generation model

The characteristics of the battery heat generated arise from the integrated effect of the internal complex electrochemical reactions and the electrical-heat transformation. During the normal operation of the battery, the total heat generation rate is mainly composed of reversible heat from electrochemical reactions, irreversible Joule heat, heat from side reactions and heat of mixing [5, 29, 30]. As is always the case, for the high power battery under consideration in the current work, the heat from side reactions and heat of mixing are small enough to be ignored [12, 23]. The temperature and SOC of the battery are assumed on only spatial variation. According to the thermal model presented by Bernardi et al. [9], the simplified heat generation model inside the battery can be described as follows:

$$q = I^2 R(I,\mathrm{SOC}) - IT\frac{\partial E(\mathrm{SOC})}{\partial T} \tag{1}$$

$$q_{\mathrm{J}} = I^2 R(I,\mathrm{SOC}) = I\big(E(\mathrm{SOC}) - U(I,t)\big) \tag{2}$$

where q is the heat generation rate, I is the charge or discharge current, which is negative in charge process and positive in discharge process, R is the direct current (DC) resistance in the battery, T is the battery temperature, E is the open-circuit potential, U is the terminal voltage, q_{J}

is the irreversible Joule heat, SOC is the state of charge, $IT\frac{\partial E}{\partial T}$ is the reversible electrochemical reactions heat. According to Eq. (1), the battery heat generation rate is the function of the ambient temperature, charge/discharge rates and DC resistance.

The irreversible Joule heat is dependent on the battery DC resistance which is not a constant. The DC resistance primarily comprises ohmic and polarization resistance [31]. The former obeying ohm's law is dependent on the material property and geometry structure of the battery but has no relationship with the SOC. The latter is caused by the polarization between the positive and negative electrode during the electrochemical reactions in the battery. Its value is dependent on the SOC and increases with the increase of the current density.

In general, during the period of high charge/discharge rates, the irreversible Joule heat dominates among the total heat generation and the reversible heat is small compared to the Joule heat [16]. Therefore, the reversible heat is often negligible and the irreversible Joule heat is considered as the heat generation rate. Obviously, such treatment will lead to the deviation from the actual value. Moreover, in order to obtain the terminal voltage variations at transient conditions as measuring the DC resistance, the data in a reasonable time interval should be selected in accordance with experience. The selection of time interval also results in errors. As a consequence, this method is not accurate as well [32].

3.2. Heat dissipation model

For the rate of heat generated in a battery, one of them is stored in the battery, also known as sensible heat. The primary heat is removed to the TMS through three kinds of well-known heat transfer mechanisms: conduction, convection and radiation. Generally, the operating temperature of most of the batteries is less than 60 ^{o}C under normal operation. Therefore, the amount of the heat radiation was small that can be ignored [33-35]. The heat dissipation of the battery is dependent on the type of the TMS. For example, in the TMS based on the liquid cooling, the heat of the battery is first conducted to the heat exchange unit and then transferred to the working fluid by convection. In the TMS, based on the heat pipes or phase change materials, the heat was removed to the working medium by conduction. However, the heat generation rate in the battery is independent of heat emission mode provided by the TMS.

In this study, an air cooling TMS is selected to build the heat dissipation mode, in which the convection is primary. Thus, according to the energy balance, the total heat generation rate can be expressed as follows:

$$\rho cV\left(T_{\mathrm{t}}-T_{0}\right)=-\int\frac{T_{\mathrm{t}}-T_{\mathrm{amb}}}{R_{\mathrm{h}}}+\Phi \tag{3}$$

where ρ is the density of the battery, c is the specific heat of the battery, V is the volume of the battery, T_{t} and T_0 are the battery temperature at the time of 0 and t, Φ is the total heat generation, R_{h} is the convective thermal resistance, T_{amb} is the ambient temperature.

3.3. Determination of heat generation rate

When taking the heat transfer inside the battery into consideration only, based on the assumptions of the uniform material, isotropic thermal properties as well as the specific heat and thermal conductivity independent of temperature, the governing thermal equation describing the battery conduction may be written:

$$\rho c\frac{\partial T}{\partial t}=\lambda\left(\frac{\partial}{\partial t}\left(\frac{\partial T}{\partial x}\right)+\frac{\partial}{\partial t}\left(\frac{\partial T}{\partial y}\right)+\frac{\partial}{\partial t}\left(\frac{\partial T}{\partial z}\right)\right)+q_{\mathrm{v}} \tag{4}$$

where q_{v} is the heat generation rate per unit cell volume, λ is the thermal conductivity of the battery cell, t is the time.

Under above assumptions, the battery cell will have a uniform internal temperature at a fixed time and can be considered as a mass point. Therefore, the lumped parameter method is efficient for solving the transient heat transfer problem of the battery [12]. In addition, the charging and discharging duration can be separated into many small time steps. If the time step size is small enough, the heat generation rate can be considered constant during this period. In the current work, the time step equals the data acquisition interval. For the air cooling TMS, the energy balance equation with its analytic solution can be described as follows:

$$\rho cV\frac{\partial T}{\partial t}=q_{\mathrm{t}}-\frac{T_{\mathrm{t}}-T_{\mathrm{amb}}}{R_{\mathrm{h}}},\quad t\leq\tau \tag{5}$$

$$t=0,\quad T=T_0 \tag{6}$$

$$\frac{q_{\mathrm{t}}R_{\mathrm{h}}-\left(T-T_{\mathrm{amb}}\right)}{q_{\mathrm{t}}R_{\mathrm{h}}-\left(T_{0}-T_{\mathrm{amb}}\right)}=\exp\left(-\frac{1}{\rho cVR_{\mathrm{h}}}t\right)=\exp\left(-\frac{1}{B}t\right) \tag{7}$$

where τ is the time step, B is the time constant that represents the response speed of the temperature variation of the battery, $B=\rho cVR_{\mathrm{h}}$. When the rate of the heat generated is equal to 0, it can be calculated by the following equations:

$$\frac{T - T_{\mathrm{amb}}}{T_0 - T_{\mathrm{amb}}} = \exp\left(-\frac{1}{B}t\right) \tag{8}$$

$$B = t \Big/ \ln\left(\frac{T_0 - T_{\mathrm{amb}}}{T - T_{\mathrm{amb}}}\right) \tag{9}$$

For the calculation of the convective thermal resistance, the steady state method is usually used. In other words, through measuring the surface temperature of heat source, ambient temperature and heating power at steady state, the convective thermal resistance can be obtained by Eq. (10):

$$R_{\mathrm{h}} = \frac{T_{\mathrm{max}} - T_{\mathrm{amb}}}{Q} \tag{10}$$

where Q is the heating power and T_{max} is the surface temperature of heat source at steady state.

The Biot number (Bi) is a dimensionless quantity, $Bi=hl/\lambda$, which denotes the ratio of the internal heat transfer resistance to the external heat transfer resistance for a body. For the lithium-ion battery, the internal heat transfer resistance is determined by its thermal conductivity. The convection thermal resistance is dependent on the convective heat transfer coefficient. As $Bi<0.1$, the temperature inside the battery is approximately uniform and is only dependent on the time. Therefore, the heat generation rate can be calculated by Eq. (11):

$$q = \frac{1}{R_{\mathrm{h}}}\left(\frac{T - T_0}{1 - \exp\left(-\frac{t}{B}\right)} + T_0 - T_{\mathrm{amb}}\right) \tag{11}$$

When the battery initial temperature, ambient temperature, the battery temperature, convective thermal resistance and physical properties of the battery are all known, the heat generation rate are also known under different SOC conditions.

Based on the battery thermal conductivity test device, the measured value of the thermal conductivity is 5.22 W/(m•K). Utilizing the relevant experimental data presented in the literature [36], the steady state temperatures of the heat source at different heating power are obtained under the natural and forced convection cooling conditions. For the forced convection cooling, the air flow rate is 18 m^3/h. The ambient temperature is set as 20 ^{o}C. According to Eq. (10), the average values of the convective resistance (R_{h}) can be achieved, which are 13.87 K/W and 2.03 K/W under the natural and forced convection cooling conditions, respectively. Consequently, Bi

can be calculated assuming that the thermal properties of the cooling air are constant in the temperature range from 20 ^{o}C to 55 ^{o}C. For the natural convection cooling, *Bi* equals 0.0043, while for the forced convection cooling, *Bi* is equal to 0.0271. This indicates that the internal heat transfer resistance of the battery can be negligible. In addition, according to the temperature drop of the battery shown in Fig. 3, the time constant can thus be calculated in terms of Eq. (9), which is approximate 6944.44 s under the natural convection at 28 ^{o}C and is approximate 1052.63 s, 1075.27 s, 1030.93 s under the forced convection with air flow rate of 18 m^3/h at 28 ^{o}C, 35 ^{o}C, 42 ^{o}C, respectively.

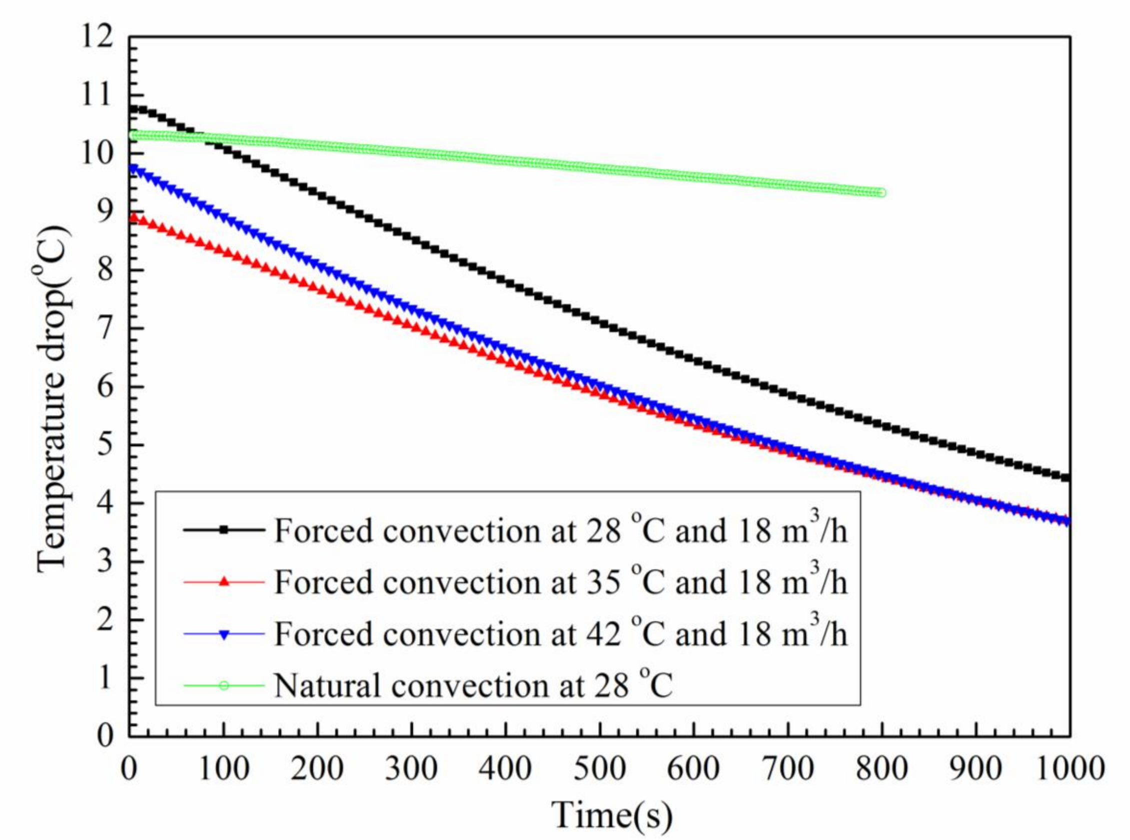

Fig. 3. Temperature drop of the battery under the natural and forced convection.

As a consequence, the calculating equations of the transient heat generation rate under the natural convection cooling and forced convection cooling at 35 ^{o}C are expressed as Eq. (12) and Eq. (13), respectively.

$$q = 0.072\left(\frac{T - T_0}{1 - \exp\left(-0.000144t\right)} + T_0 - T_{\text{amb}}\right) \tag{12}$$

$$q = 0.493\left(\frac{T - T_0}{1 - \exp\left(-0.00093t\right)} + T_0 - T_{\text{amb}}\right) \tag{13}$$

Fig. 4 presents the calculated value of the heat generation rate in the 4C discharge process at ambient temperature of 35 ^{o}C under natural convection and forced convection with air flow rate of 18 m^3/h. As can be seen from Fig. 4, both curves show a nearly same trend of change, which indicates that the cooling way has little influence on the heat generation rate of the battery. The deviation from each other during the period of 600 s to 800 s may be caused by the difference of the battery temperature between under natural convection and forced convection. The same conclusion can be obtained by Eq. (1), that is, the heat generation rate is only dependent on the battery temperature, DC resistance and charge/discharge rates.

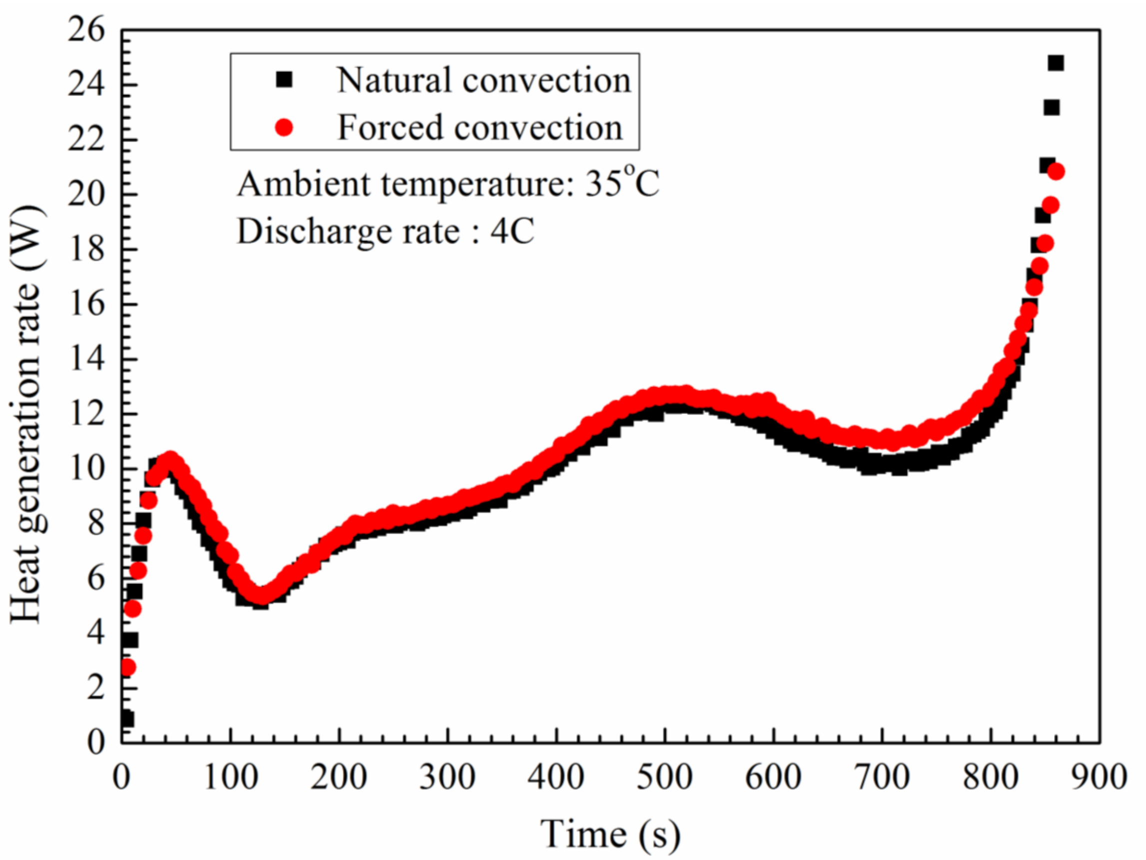

Fig. 4. Comparison of heat generation rate under the natural and forced convection.

3.4 Model validation

For the purpose of validating the model, an integrated thermal management system (ITMS) with paraffin phase change material and air cooling is designed for the lithium-ion battery. Experimental and simulating investigations on the performance of the ITMS are carried out. The details of the ITMS of the battery can be referred to the literature [36]. Furthermore, the simulation model of the battery with the ITMS is set up and the temperature of the battery is simulated based on the commercial FLUENT software.

Fig. 5 shows the comparison between the simulated and experimental battery temperatures for the case of 4C charge/discharge processes under ambient temperature of 35 °C condition. As shown in Fig. 5, it can be clearly seen that the battery temperatures simulated is in good agreement with those measured. The maximum error is 2.1% in charge process and is 1.3% in discharge process. The results demonstrate that the heat generation rate model is robust and accuracy.

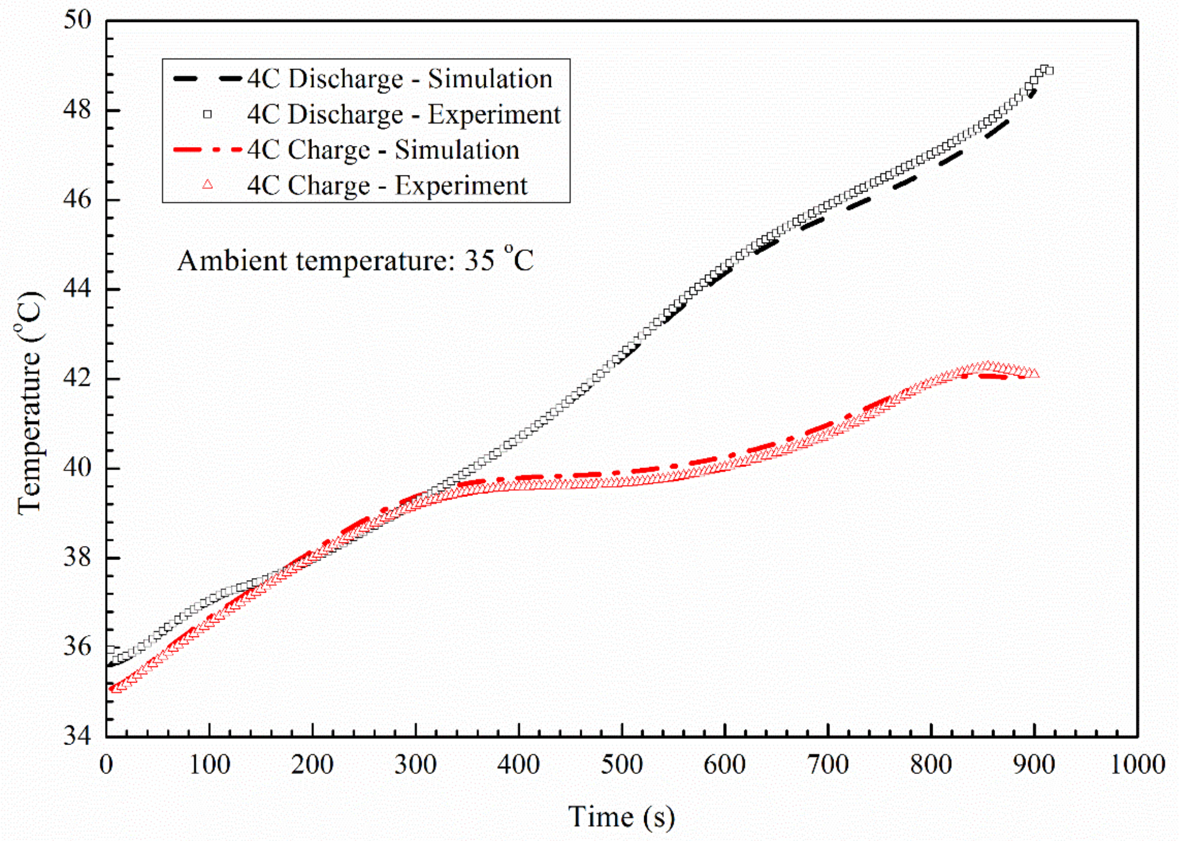

Fig. 5. Comparison of simulated and experimental battery temperatures at 4C charge/discharge rate and ambient temperature of 35 °C.

4. Results and discussion

According to Eq. (1), the ambient temperature and charge/discharge rate have significant effect on the heat generation rate, the charge/discharge characteristics and temperature rise behavior of single cell. Therefore, in this section, the impact on the charge/discharge characteristics is analyzed firstly. Then the impact on the temperature rise of a single cell and the heat generation rate are discussed in detail.

4.1. Impact on battery charge/discharge characteristics

Fig. 6 depicts the terminal voltage profiles of the battery under the discharge rates of 2C, 3C and 4C at ambient temperature of 28 °C as well as at ambient temperatures of 28 °C, 35 °C and 42 °C during 2C discharge. As can be seen from Fig. 6, the higher the discharge rate, the larger the descent rate of the terminal voltage of the battery. As the ambient temperature is higher, the descent rate of the terminal voltage is smaller, but the discharge time is longer.

In Fig. 6(a), the battery terminal voltage decreases with the increase of DOD. As DOD exceeds 0.9, the terminal voltage drops rapidly. The irreversible Joule heat is proportional to the descent rate of the terminal voltage and discharge rate in terms of Eqs. (1) and (2). Therefore, a larger amount of heat is generated in the battery under high-rate discharge conditions. Moreover, the battery temperature is larger in the discharge process when the ambient temperature is higher.

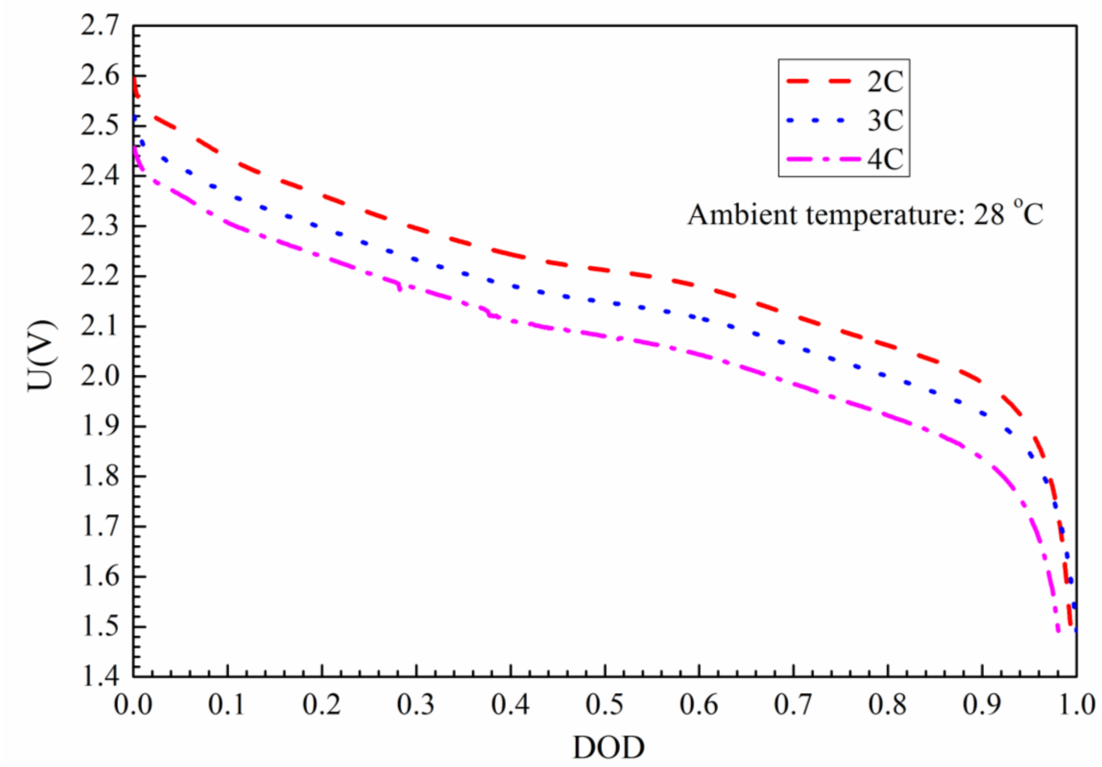

(a) Under 2C, 3C and 4C discharge rates at 28 °C

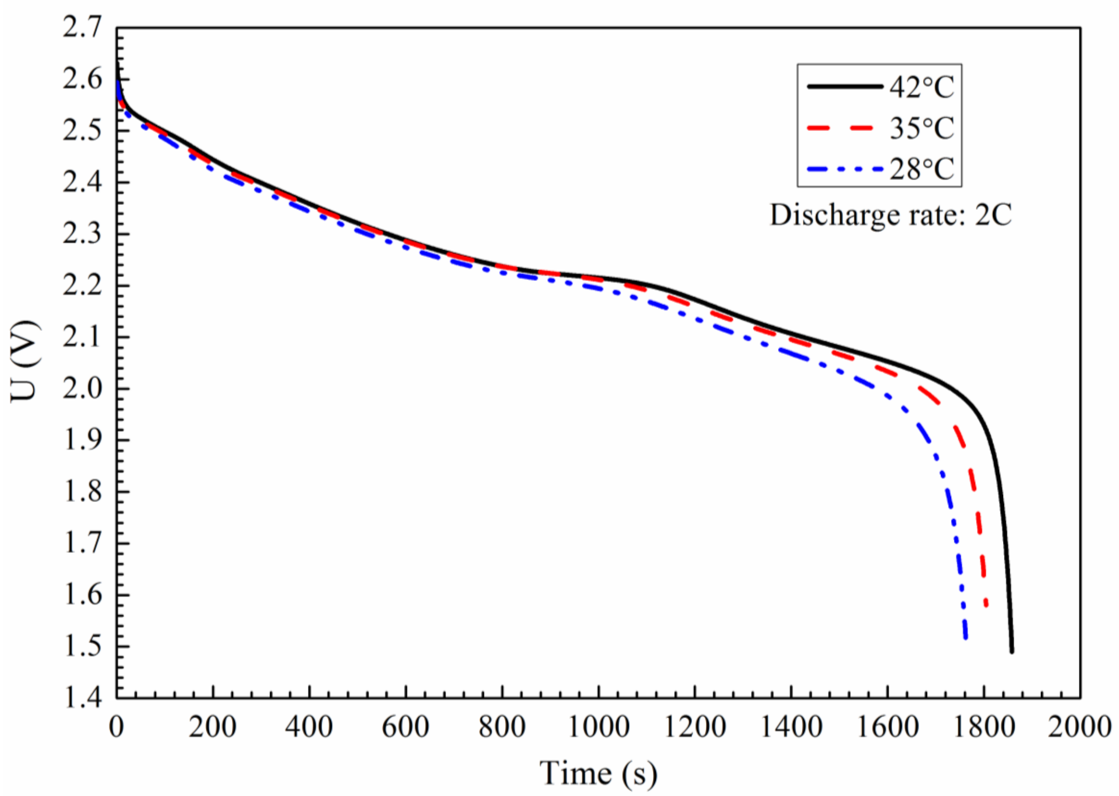

(b) Under 28 °C, 35 °C and 42 °C at 2C discharge rate

Fig. 6. Terminal voltage profiles under 2C, 3C and 4C discharge rates as well as 28 °C, 35 °C and 42 °C ambient temperature.

As shown in Fig. 6(b), it can be found that the terminal voltage has no obvious change under different ambient temperature for 2C discharge rate when the discharge time is less than 1000 s. The main reason could be that there is a very small difference among the battery temperatures under 28 °C, 35 °C, and 42 °C conditions during these periods. As the discharge time is more than 1000 s, the effect of the ambient temperature on the discharge characteristics starts to be remarkable. What's more, the discharge time is longer when the ambient temperature is higher. It could be explained by the fact that the electrochemical reactions are improved by the higher battery temperature. At the same time, the DC resistance decreases and this further decreases the electrical loss. As a consequence, the heat generation rate is small as the ambient temperature is high.

In addition, it is worth noting that there are similar behaviors under 2C charge rate with those under 2C discharge rate, that is, the higher the charge rate, the larger the ascent rate of the terminal voltage of the battery. As the ambient temperature is higher, the ascent rate of the terminal voltage is smaller, but the time for charging is longer.

4.2. Impact on battery temperature rise behavior

Considering the temperature rise behavior of the single cell is due to its heat generation, the experimental investigations on the temperature rise behavior are carried out under the room temperature of 24.1 ^{o}C during the period of 1C, 2C, 3C and 4C charge/discharge, as shown in Fig. 7. It can be seen from Fig. 7 that the curves of the temperature rise demonstrate obvious differences between the charge process and discharge process. As is expected, two peaks are observed for temperature rise curves during the period of low-rates charge (1C and 2C). It is also noted that the temperature rise in the charge process is less than that in the discharge process. As a consequence, the charge/discharge rates have remarkable influences on the temperature rise of the battery cell. Moreover, it should be stress here that the temperature rise infers the battery temperature beyond the ambient temperature.

In Fig. 7(a), the slopes of the curves of the battery temperature rise are significantly different from each other under different discharge rates conditions. If the initial temperatures are same, the higher the discharge rate after the battery begins to discharge, the higher the rate of the temperature rise, which indicates that the heat generation rate increases along with the increase of the discharge rate. During the period of 1C, 2C 3C and 4C discharge, the maximum values of the temperature rise are 7.3 ^{o}C, 9.6 ^{o}C, 13.0 ^{o}C and 15.5 ^{o}C, respectively.

Compared with the results shown in Fig. 7(a), the rates of the temperature rise in Fig. 7(b) are obviously lower than those corresponding values under the same charge/discharge rate conditions. The maximum temperature rises in the processes of 1C, 2C, 3C and 4C charge rates are 2.7 ^{o}C, 4.1 ^{o}C, 6.8 ^{o}C and 9.4 ^{o}C, respectively. This indicates that the heat generation rate for the charge process is much lower than that in the discharge process. Furthermore, during the period of the charge there are obvious fluctuations for the curves of the temperature rise, especially at low charge rates.

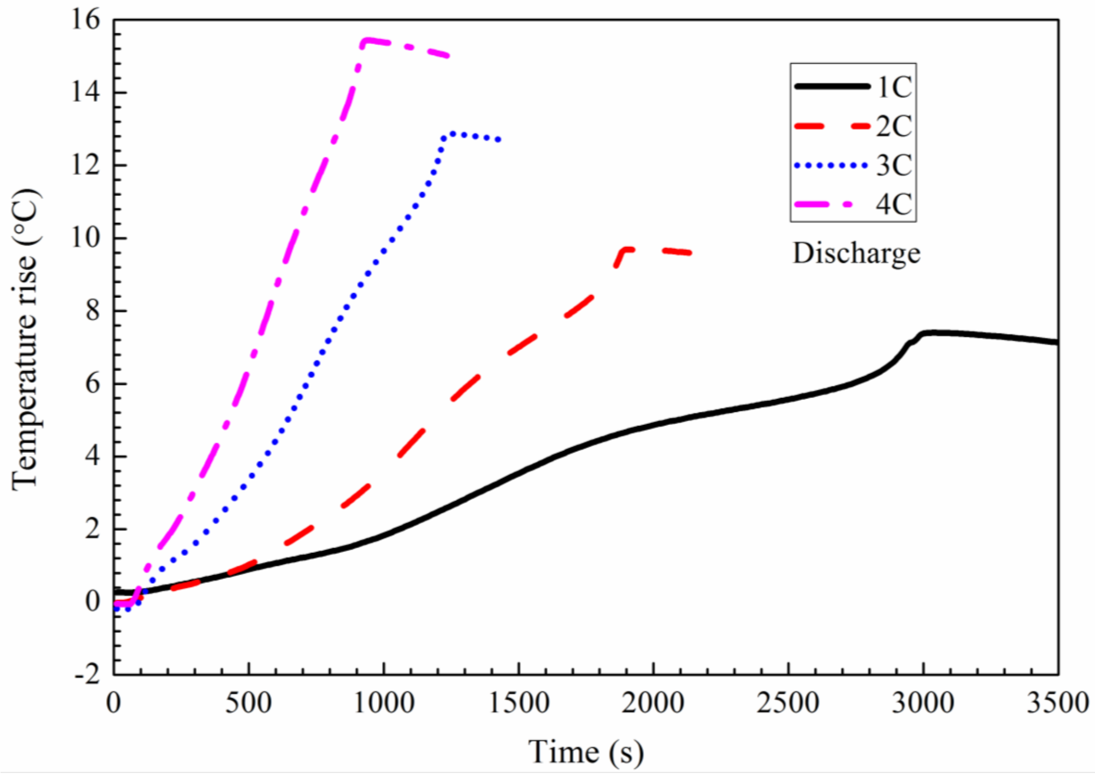

(a) Discharge

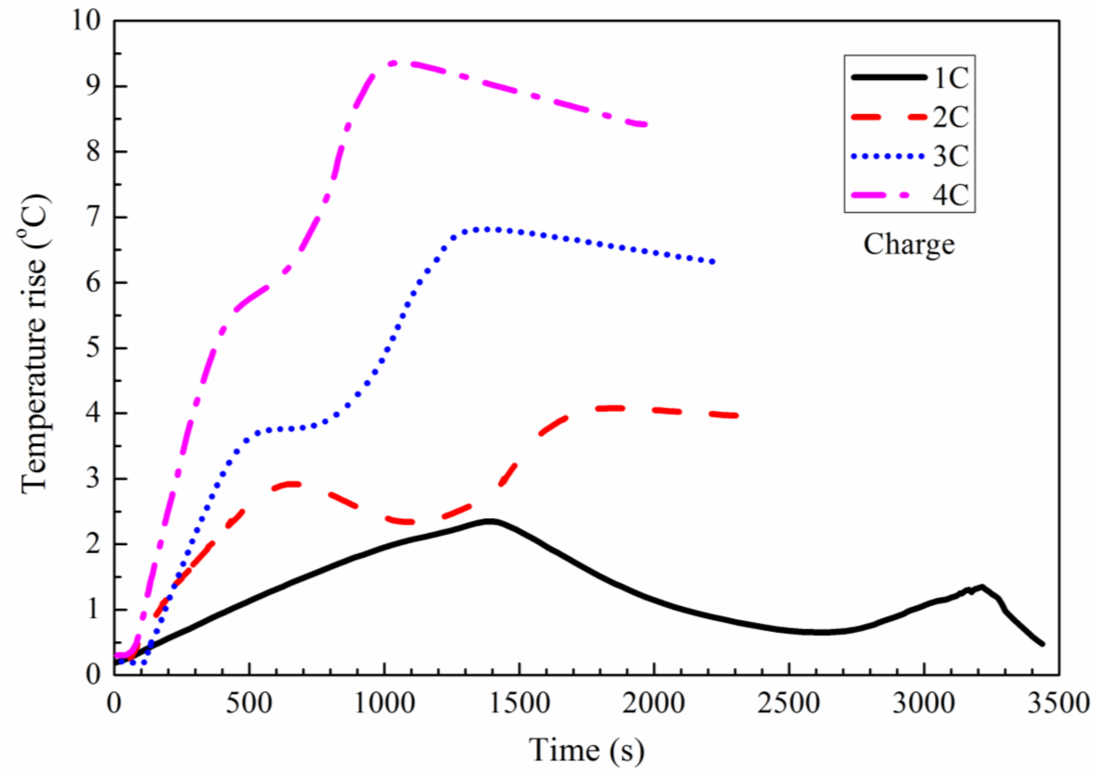

(b) Charge

Fig. 7. Temperature rise profiles during 1C, 2C, 3C and 4C discharge/charge rates at 24.1 ºC.

In the early stage of the charge, the battery is heated up quickly because the battery temperature and ambient temperature are close and the convective heat dissipation is small. In the middle stage of the charge, the battery temperature is significantly reduced during 1C and 2C charge rates, because the heat generation rate of the battery is less than the heat dissipation rate. While in 3C and 4C charge processes, the battery heat generating rate is close to dissipation rate, resulting in a non-obvious temperature increase. At the end stage of the charge, the battery DC resistance increases under the large SOC conditions, leading to an increase in the irreversible Joule heat. Therefore, the battery temperature rises again.

For the influence of ambient temperature on the temperature rise of the single cell, Table 2 illustrates the maximum temperature rises at the ambient temperatures of 28 ^{o}C, 35 ^{o}C, 42 ^{o}C in the 2C, 3C and 4C discharge processes, respectively. As can be seen clearly from Table 2, at a fixed ambient temperature, the larger the discharge rate, the larger the maximum temperature rise of the battery. Moreover, for a fixed discharge rate, the higher the ambient temperature, the lower the maximum temperature rise of the battery. The primary reason for this result is the difference of the battery temperature under different ambient temperature conditions. Consequently, the ambient temperature has a remarkable impact on the heat generation rate, which decreases with increased ambient temperature. For the 4C discharge process, the maximum temperature rise of the battery is approximate 16.5 ^{o}C at the ambient temperature of 28 ^{o}C and around 12.7 ^{o}C at the ambient temperature of 42 ^{o}C.

Table 2 Maximum temperature rise under different ambient temperatures and discharge rates conditions.

Ambient temperature (^{o}C)	28	35	42
$\mathit{\Delta} T_{\max}$ at 2C discharge rate	11.3	10.2	9.8
$\mathit{\Delta} T_{\max}$ at 3C discharge rate	13.6	12.8	11.7
$\mathit{\Delta} T_{\max}$ at 4C discharge rate	16.5	13.3	12.7

4.3. Impact of charge/discharge rate on heat generation rate

Fig. 8 depicts the profiles of the heat generation rate under the ambient temperature of 35 ^{o}C and the charge/discharge rates of 2C, 3C and 4C. It can be found that there is a great difference for the heat generation rate in the 2C, 3C and 4C charge/discharge processes. A greater charge/discharge rate gives rise to a greater heat generation rate, which matches the analytic results in Section 4.1 and Eq. (1).

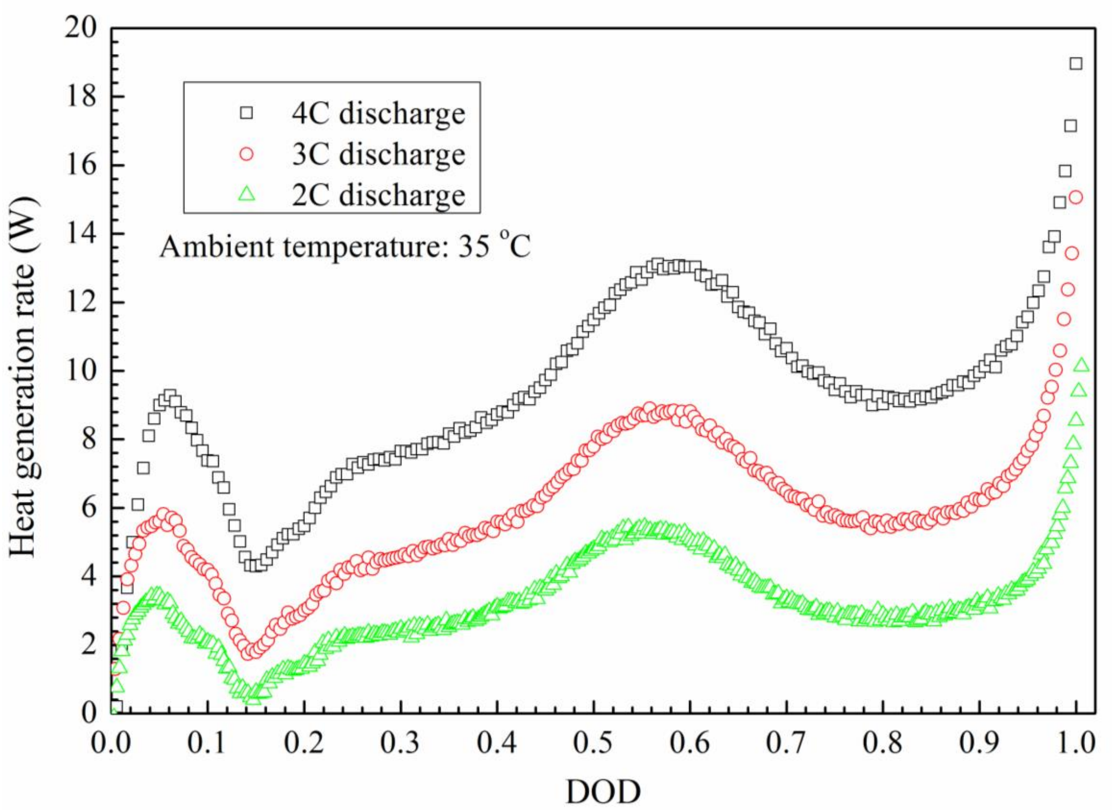

(a) Discharge

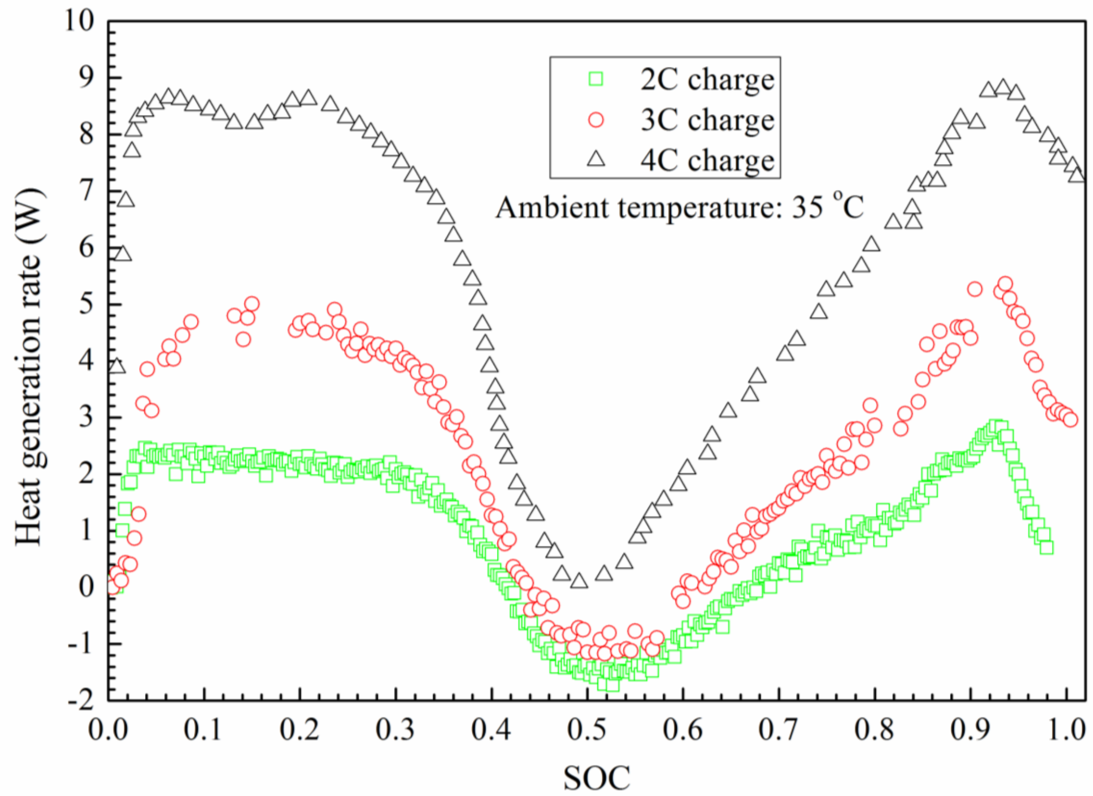

(b) Charge

Fig. 8. Comparison of heat generation rate at 35 ^{o}C under 2C, 3C and 4C discharge/charge rates

According to the results shown in Fig. 8(a), the heat generation rate in the discharge process can be divided into five different stages. When DOD is equal to 0.05, 0.55 and 1.0, respectively, the heat generation experiences three obvious peaks. When the discharge process begins, the heat generation rate increases rapidly, and it reaches a peak value at DOD=0.05. Meanwhile the peak rates for the 4C, 3C and 2C discharge are 9.3 W, 5.8 W and 3.4 W, respectively. When $0.05<DOD<0.55$, the heat generation rate slightly decreases at first, then gradually increases and reaches the second peak at DOD=0.55. At this time, the peak rates are 13.1W, 8.7W and 5.4W during the 4C, 3C and 2C discharge, respectively. As DOD ranges from 0.6 to 0.9, the heat generation rate gradually decreases. When the discharge process is nearly completed ($DOD>0.9$), the heat generation rate rises sharply, and reaches the maximum at the end of the discharge process. The maximum rates during the 4C, 3C and 2C discharge are 18.9 W, 15.0 W and 10.1 W, respectively. Consequently, the sharp increase of heat generation rate easily caused the battery beyond its allowable temperature potentially. Thus the overdischarge ($DOD>0.9$) should be avoided in the actual applications.

As can be seen from Fig. 8(b), there is an obvious distinction for the heat generation rate in the charge process in comparison with that in the discharge process. Under different charge/discharge rates, the battery heat generated exhibits a M-shaped curve in general. The average heat generation rate for charge process is lower than that for discharge process under the same current rate conditions. When SOC= 0.05 and SOC= 0.9, the battery has two obvious peak rates, and they are close to each other. When SOC is between 0.05 and 0.3, the heat generation rate change in the charge process is relatively small.

When SOC= 0.55, the heat generation curve has obvious valley. At this moment, the minimum heat generation rate for the 4C, 3C, and 2C charge rates are 0.1 W, -0.9 W, and -1.6 W, respectively. The heat generation rate includes irreversible Joule heat and reversible reaction heat. The irreversible Joule heat depends on the charge rate and the DC resistance, which is constantly positive, whereas the reaction heat during charge process is constantly negative. The heat generation rate appears as negative for charge process of 2C and 3C, indicating that at this stage the heat absorption of electrochemical reaction is greater than irreversible Joule heat. However, the heat generation rate for 4C rate is not negative, indicating that the greater charge rate can lead to a larger proportion of irreversible Joule heat in total heat generated. When SOC is greater than 0.9, the heat generation rate is rapidly reduced, mainly due to the conversion from constant current charging to constant voltage charging, resulting in the battery charge current rapidly reduced.

In addition, the variation curves of the heat generation rate in the charge/discharge processes are basically consistent with the trend of the battery temperature change shown in Fig. 7. As the charge/discharge rates are large, the slope of the temperature rise curve is large and the rate of the temperature rise is high. For the cases of 1C and 2C discharge processes, the temperature rise is very small during the initial period due to the small heat generation rate, as shown in Fig. 7(a) and Fig. 8(a). Along with the increase of the discharge time, the increasing heat generation rate leads to a larger temperature rise. For the 3C and 4C discharge processes, the temperature rise is obviously larger due to the higher heat generation rate. However, for the case of charge process, the rapid increase of the heat generation rate can result in the larger temperature rise in the initial period of the charge compared with the discharge process, as shown in Fig. 7(b) and Fig. 8(b). During the middle stage, the notable decrease of the heat generation rate could result in the temperature rise obviously changing, especially at 1C and 2C charge rates.

4.4. Impact of ambient temperature on heat generation rate

The impact of the ambient temperature on the heat generation rate is mainly reflected in three aspects, i.e. in addition to the battery temperature and DC resistance, the heat generated by electrochemical reactions in the battery during the period of charge/discharge. In order to evaluate the heat generation rate under different ambient temperatures, the heat generation rates are calculated in terms of Eq. (12) for 3C charge/discharge processes and ambient temperature of 28 ^{o}C, 35 ^{o}C and 42 ^{o}C, as shown in Fig. 9. It can be seen clearly that the curves of the heat generated show the same change trend for the charge or discharge process under different ambient temperatures. The average heat generation rate in the 3C charge process is smaller than that in 3C discharge process.

For the 3C discharge process, as shown in Fig. 9(a), as the DOD is less than 0.65, the change of the heat generation rate under different ambient temperatures show a nearly same trend and a very small difference of the heat generated is presented. The heat generated at 28 ^{o}C is slightly larger than that at 35 ^{o}C and 42 ^{o}C. Conversely, when the DOD is more than 0.65, the heat generation rate presents an obvious distinction from each other. Moreover, the heat generation rate decreases as the ambient temperature increases. The results are consistent with the battery temperature rise shown in Table 2. In addition, the curves of the heat generation rate also show three peaks under different ambient temperatures. It is at the nearly same DOD that the peak appears for every ambient temperature.

For the 3C charge process, it can be concluded from Fig. 9(b) that the higher the ambient temperature, the smaller the battery heat generation rate. Under different ambient temperatures conditions the battery heat generated exhibits generally a M-shaped curve. During the initial period of charging, the heat generation rate sharply increases and reaches a peak value. At the intermediate states of the charge, the heat generated has a great depression and the minimal value of -3 W reached as SOC is approximate 0.53. It is approximately at SOC=0.9 that a peak power reaches again. Furthermore, under different ambient temperatures, the difference in heat generation rate mainly appears near the peak and valley regions, while in the SOC intervals of 0.2 to 0.4 and 0.6 to 0.8, the heat generation rate only appears a small difference.

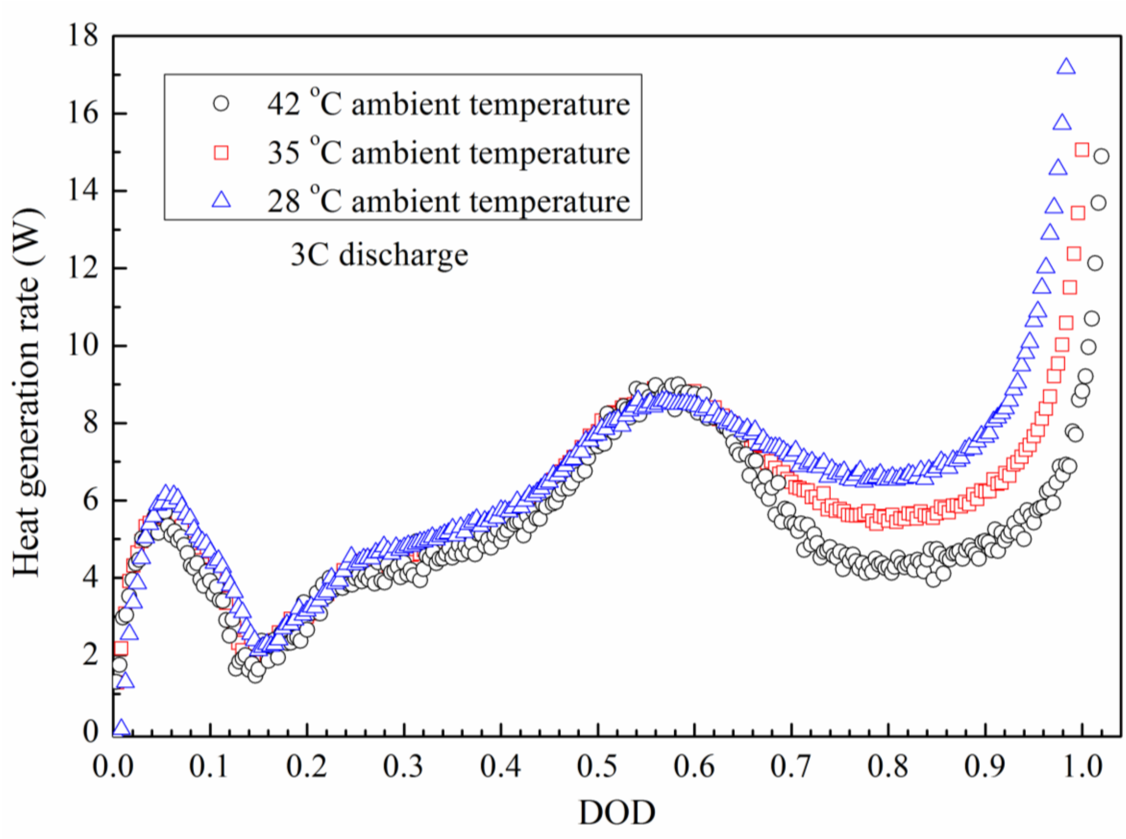

(a) Discharge

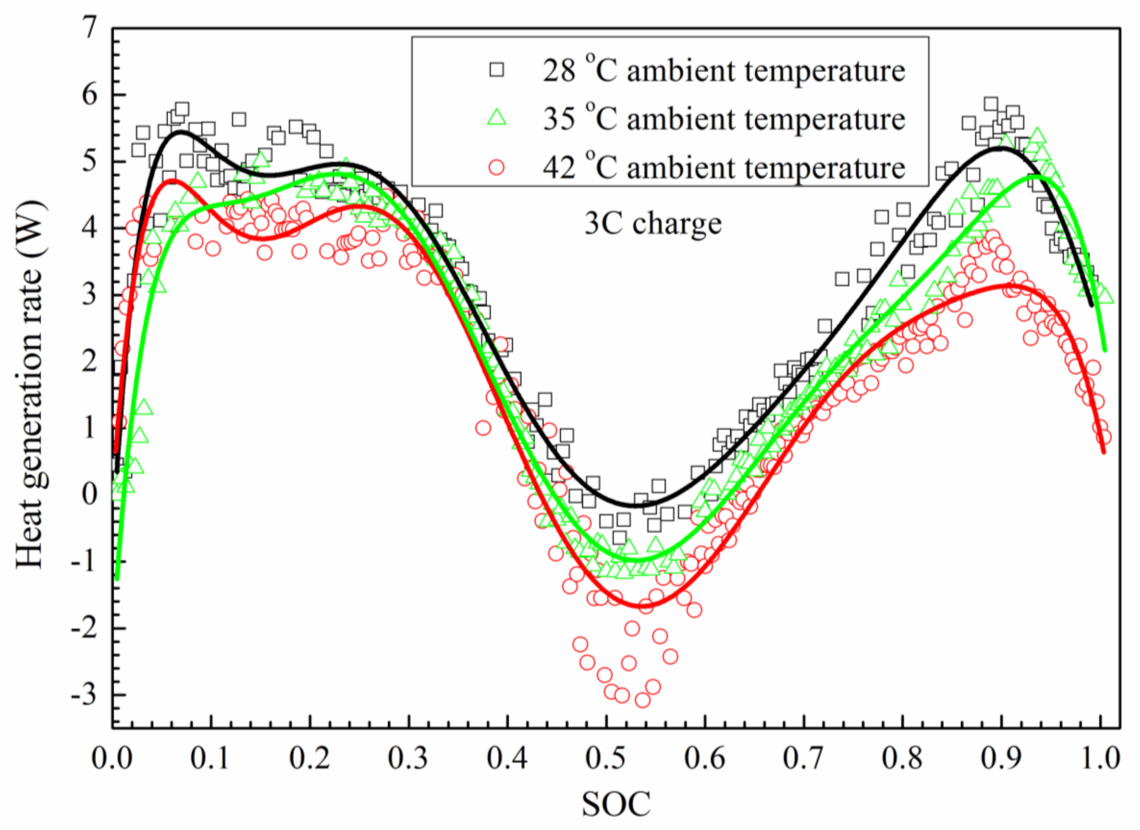

(b) Charge

Fig. 9. Comparison of heat generation rate at 3C discharge/charge under different ambient temperatures.

5. Conclusions

In this study, the transient heat generation characteristics of the lithium-ion power battery are investigated experimentally and analytically. The lumped parameter model for the heat generation rate is newly developed based on the air cooling TMS. The heat generation characteristics experimental setup is built. The model is validated by comparing the simulated battery temperatures with experimental results and good agreement is achieved. The impacts of the ambient temperatures and charge/discharge rates on the charge/discharge characteristics, the temperature rise behavior and the heat generation rate are analyzed in a systemic manner. The main conclusions can be stated as follows:

(1) The measured thermal conductivity for single cell is 5.22 W/(m•K). The expression of the transient heat generation rate is presented.

(2) Over the period of charge and discharge, the higher the charge/discharge rate, the larger the heat generation rate. High charge/discharge rate (4C) has great influence on the terminal voltage change.

(3) The heat generation curves show an obvious difference between in the charge/discharge process. The heat generation rate reaches the maximum value at DOD=1.0 and rises sharply caused by overdischarge. The rate of heat generated for the charge process exhibits a M-shaped curve. The negative heat generation rate appears at the intermediate state and results in the battery temperature rapid decrease.

(4) As DOD is less than 0.55, the ambient temperature has no obvious impact on the heat generation rate, while DOD is more than 0.55, the higher the ambient temperature, the lower the heat generation rate. In the charge process, the heat generation rate shows small distinctions for SOC ranged from 0.2 to 0.4 and from 0.6 to 0.8. Moreover, the higher the ambient temperature, the longer the charge/discharge time.

Acknowledgement

The authors would like to thank for support of this work by the CRRC TANGSHAN CO., LTD. China and financial support from University of Hertfordshire.

References

[1] B. Dunn, H. Kamath, J. M. Tarascon, Electrical energy storage for the grid: a battery of choices, Science 334 (6058) (2011) 928-935.

[2] S. Abada, G. Marlair, A. Lecocq, M. Petit, V. Sauvant-Moynot, F. Huet, Safety focused modeling of lithium-ion batteries: A review, Journal of Power Sources 305 (2016) 178-192.

[3] M. Mathew, Q. H. Kong, J. McGrory, M. Fowler, Simulation of lithium ion battery replacement in a battery pack for application in electric vehicles, Journal of Power Sources 349 (2017) 94-104.

[4] J. M. Tarascon, M. Armand, Issues and challenges facing rechargeable lithium batteries, Nature 414 (6861) (2001) 359-367.

[5] Q. S. Wang, Q. J. Sun, P. Ping, X. J. Zhao, J. H. Sun, Z. J. Lin, Heat transfer in the dynamic cycling of lithium–titanate batteries, International Journal of Heat and Mass Transfer 93 (2016) 896-905.

[6] Q. Wang, B. Jiang, B. Li, Y. Yan, A critical review of thermal management models and solutions of lithium-ion batteries for the development of pure electric vehicles, Renewable and Sustainable Energy Reviews 64 (2016) 106-128.

[7] X. Duan, G. F. Naterer, Heat transfer in phase change materials for thermal management of

electric vehicle battery modules, International Journal of Heat and Mass Transfer, 53 (23-24) (2010) 5176-5182.

[8] N. Javani, I. Dincer, G. F. Naterer, B. S. Yibas, Heat transfer and thermal management with PCMs in a Li-ion battery cell for electric vehicles, International Journal of Heat and Mass Transfer, 72 (2014) 690-703.

[9] D. Bernardi, E. Pawlikowski, J. Newman, A general energy balance for battery systems, Journal of the Electrochemical Society 132 (1984) 5-12.

[10] L. Rao, J. Newman, Heat-generation rate and general energy balance for insertion battery systems, Journal of the Electrochemical Society 144 (1997) 2697-2704.

[11] H. J. Dong, S. M. Baek, Thermal modeling of cylindrical lithium ion battery during discharge cycle, Energy Conversion and Management 52 (2011) 2973-2981.

[12] C. Forgez, D. V. Do, G. Friedrich, M. Morcrette, C. Delacourt, Thermal modeling of a cylindrical $LiFePO_4$/graphite lithium-ion battery, Journal of Power Sources 195 (2010) 2961-2968.

[13] N. Sato, Thermal behavior analysis of lithium-ion batteries for electric and hybrid vehicles, Journal of Power Sources 99 (2000) 70-77.

[14] Y. Lai, S. Du, L. Ai, L. Ai, Y. Cheng, Y. Tang, M. Jia, Insight into heat generation of lithium ion batteries based on the electrochemical-thermal model at high discharge rates, International Journal of Hydrogen Energy 40 (2015) 13039-13049.

[15] M. Yildiz, H. Karakoc, I. Dincer, Modeling and validation of temperature changes in a pouch lithium-ion battery at various discharge rates, International Communications in Heat and Mass Transfer 75 (2016) 311-314.

[16] K. Somasundaram，E. Birgersson，A. S. Mujumdar, Thermal-electrochemical model for passive thermal management of a spiral-wound lithium-ion battery, Journal of Power Sources 203 (2012) 84-96.

[17] M. Xiao, S. Y. Choe, Theoretical and experimental analysis of heat generations of a pouch type $LiMn_2O_4$/carbon high power Li-polymer battery, Journal of Power Sources 241 (2013) 46-55.

[18] S. A. Hallaj, J. Prakash, J. R. Selman, Characterization of commercial Li-ion batteries using electrochemical–calorimetric measurements, Journal of Power Sources 87 (2000)

186-194.

[19] A. Q. Yasir, T. Laurila, J. Karppinen, K. Jalkanen, K. Vuorilehto, L. Skogström, M. P. Kröckel, Heat generation in high power prismatic Li-ion battery cell with $LiMnNiCoO_2$ cathode material, International Journal of Energy Research 38 (2014) 1424-1437.

[20] M. Balasundaram, V. Ramar, C. Yap, L. Li, A. A. Tay, P. Balaya, Heat loss distribution: Impedance and thermal loss analyses in $LiFePO_4$/graphite 18650 electrochemical cell, Journal of Power Sources 328 (2016) 413-421.

[21] Y. Saito, Thermal behaviors of lithium-ion batteries during high-rate pulse cycling, Journal of Power Sources 146 (2005) 770-774.

[22] N. Damay, C. Forgez, M. P. Bichat, G. Friedrich, Thermal modeling of large prismatic $LiFePO_4$ /graphite battery. Coupled thermal and heat generation models for characterization and simulation, Journal of Power Sources 283 (2015) 37-45.

[23] T. M. Bandhauer, S. Garimella, T. F. Fuller, Temperature-dependent electrochemical heat generation in a commercial lithium-ion battery, Journal of Power Sources 247 (2014) 618-628.

[24] S. Panchal, I. Dincer, M. Agelin-Chaab, R. Fraser, M. Fowler, Experimental and theoretical investigations of heat generation rates for a water cooled $LiFePO_4$, battery, International Journal of Heat and Mass Transfer 101 (2016) 1093-1102.

[25] S. Panchal, I. Dincer, M. Agelin-Chaab, R. Fraser, M. Fowler, Transient electrochemical heat transfer modeling and experimental validation of a large sized $LiFePO_4$/graphite battery, International Journal of Heat and Mass Transfer 109 (2017) 1239-1251.

[26] M. Farag, H. Sweity, M. Fleckenstein, S. Habibi, Combined electrochemical, heat generation, and thermal model for large prismatic lithium-ion batteries in real-time applications, Journal of Power Sources 360 (2017) 618-633.

[27] C. Zhang, K. Li, J. Deng, S. Song, Improved realtime state-of-charge estimation of LiFePO4 battery based on a novel thermoelectric model, IEEE Transactions on Industrial Electronics 64 (2017) 654-663.

[28] Y. He, Rapid thermal conductivity measurement with a hot disk sensor: Part 1. Theoretical considerations, Thermochimica acta 436 (2005) 122-129.

[29] Q. Huang, M. Yan, Z. Jiang, Thermal study on single electrodes in lithium-ion battery,

Journal of Power Sources, 156 (2006) 541-546.
[30] K. Onda, T. Ohshima, M. Nakayama, K. Fukuda, Thermal behavior of small lithium-ion battery during rapid charge and discharge cycles, Journal of Power sources 158 (2006) 535-542.
[31] M. Ouyang, Z. Chu, L. Lu, J. Li, X. Han, X. Feng, G. Liu, Low temperature aging mechanism identification and lithium deposition in a large format lithium iron phosphate battery for different charge profiles, Journal of Power Sources 286 (2015) 309-320.
[32] Z. He, G. Yang, L. Lu, A parameter identification method for dynamics of lithium iron phosphate batteries based on step-change current curves and constant current curves, Energies 9 (2016) 444-454.
[33] J. Zhao, Z. Rao, Y. Li, Thermal performance of mini-channel liquid cooled cylinder based battery thermal management for cylindrical lithium-ion power battery, Energy Conversion and Management 103 (2015) 157-165.
[34] Y. Huo, Z. Rao, X. Liu, J. Zhao, Investigation of power battery thermal management by using mini-channel cold plate[J]. Energy Conversion & Management, 2015, 89:387-395.
[35] N. Putra, B. Ariantara, R. A. Pamungkas, Experimental investigation on performance of lithium-ion battery thermal management system using flat plate loop heat pipe for electric vehicle application , Applied Thermal Engineering 99 (2016) 784-789.
[36] S. Shi, Y. Q. Xie, M. Li, Y. P. Yuan, J. Z. Yu, H. W. Wu, B. Liu, N. Liu, Non-steady experimental investigation on an integrated thermal management system for power battery with phase change materials, Energy Conversion and Management 138 (2017) 84-96.